Published in final edited form as:
Cell Rep. 2017 May 30; 19(9): 1819–1831. doi:10.1016/j.celrep.2017.05.016.

Replication-Coupled Dilution of H4K20me2 Guides 53BP1 to Pre-replicative Chromatin

Stefania Pellegrino[#1], **Jone Michelena**[#1], **Federico Teloni**[1], **Ralph Imhof**[1], and **Matthias Altmeyer**[1,3,*]

[1]Department of Molecular Mechanisms of Disease, University of Zurich, CH-8057 Zurich, Switzerland

[#] These authors contributed equally to this work.

Summary

The bivalent histone modification reader 53BP1 accumulates around DNA double-strand breaks (DSBs), where it dictates repair pathway choice decisions by limiting DNA end resection. How this function is regulated locally and across the cell cycle to channel repair reactions toward non-homologous end joining (NHEJ) in G1 and promote homology-directed repair (HDR) in S/G2 is insufficiently understood. Here, we show that the ability of 53BP1 to accumulate around DSBs declines as cells progress through S phase and reveal that the inverse relationship between 53BP1 recruitment and replicated chromatin is linked to the replication-coupled dilution of 53BP1's target mark H4K20me2. Consistently, premature maturation of post-replicative chromatin restores H4K20me2 and rescues 53BP1 accumulation on replicated chromatin. The H4K20me2-mediated chromatin association of 53BP1 thus represents an inbuilt mechanism to distinguish DSBs in pre- versus post-replicative chromatin, allowing for localized repair pathway choice decisions based on the availability of replication-generated template strands for HDR.

Introduction

In order to maintain genome stability, cells must repair DNA lesions efficiently and with greatest precision. DNA double-strand breaks (DSBs) are among the most dangerous DNA lesions, because they can disintegrate the genome. Several dedicated repair pathways have thus evolved to sense DSBs and coordinate DSB repair with other vital cellular functions. While re-ligation by non-homologous end joining (NHEJ) works independently of a template DNA strand and is therefore the pathway of choice during the G1 phase of the cell cycle, homology-directed repair (HDR) uses homologous DNA sequences and functions primarily in S/G2, when sister chromatids are available (Ceccaldi et al., 2016).

[*]Correspondence: matthias.altmeyer@uzh.ch.
[3]Lead Contact

Author Contributions

S.P., J.M., F.T., and R.I. performed experiments and analyzed results. M.A. conceived the study, supervised the work, and wrote the manuscript draft. All authors discussed the results and read and edited the final manuscript.

Europe PMC Funders Author Manuscripts

DNA end resection is a prerequisite for HDR, and the extent to which resection is allowed can determine the choice between HDR and NHEJ (Chapman et al., 2012b). A key regulator of DNA end resection at DSBs is the chromatin reader 53BP1 (Panier and Boulton, 2014; Zimmermann and de Lange, 2014). Through its accumulation around DSBs and the recruitment of various effector proteins, 53BP1 limits end resection and thereby dictates repair pathway choice decisions. Indeed, 53BP1 accumulation around DNA lesions into ionizing radiation (IR)-induced foci (IRIF) is inversely proportional to the extent of DNA end resection (Ochs et al., 2016), suggesting that the amount of 53BP1 on damaged chromatin must be tightly regulated to restore genome integrity with minimal repair-associated mutagenicity.

A prerequisite for 53BP1 recruitment is the activation of two ubiquitin ligases, RNF8 and RNF168 (Schwertman et al., 2016). Following DSB-induced ATM activation and phosphorylation of the histone variant H2AX, RNF8 ubiquitylates linker histone H1 to recruit RNF168, which in turn ubiquitylates H2AK15 (Gatti et al., 2012; Mattiroli et al., 2012; Thorslund et al., 2015). Through a recently uncovered ubiquitination-dependent recruitment (UDR) motif, 53BP1 directly binds to the DSB-induced and RNF168-mediated ubiquitylation on H2AK15 (Fradet-Turcotte et al., 2013). The localized RNF8/RNF168-mediated chromatin ubiquitylation thus ensures that 53BP1 accumulates specifically on chromatin in the vicinity of DSB sites (Altmeyer and Lukas, 2013; Gudjonsson et al., 2012). In addition, 53BP1 contains a tandem tudor domain, which in vitro work has shown to confer micromolar affinity for H4K20me2 (Botuyan et al., 2006; Greeson et al., 2008), making 53BP1 a bivalent histone mark reader (Fradet-Turcotte et al., 2013) whose mode of interaction with modified nucleosomes was recently solved at the structural level by cryoelectron microscopy (cryo-EM) (Wilson et al., 2016). Despite this biochemical characterization, it has remained unclear why the genome caretaker 53BP1 evolved to simultaneously bind two distinct histone marks, H2AK15ubi and H4K20me2. While current models propose that H4K20me2 either becomes more accessible in chromatin surrounding DSBs to promote 53BP1 recruitment (Acs et al., 2011; Mallette et al., 2012), or is enhanced upon DNA damage (Dulev et al., 2014; Pei et al., 2011; Tuzon et al., 2014), whether and how this abundant histone mark is involved in modulating 53BP1-centered repair pathway choice decisions as cells progress through S phase is not well understood.

Here we use high-content microscopy-based cell cycle staging of asynchronously growing cell populations to show that the ability of 53BP1 to accumulate around DSBs gradually declines as cells progress from early to late S phase. We further show that the reduced affinity of 53BP1 and its downstream effector RIF1 for damaged chromatin is tightly linked to the dilution of the H4K20me2 mark as cells replicate their genome and that premature chromatin maturation can restore 53BP1 accumulation on replicated chromatin. Replication-coupled alterations in the H4K20 methylation status therefore regulate DSB repair pathway choice in at least two cooperative ways: through recruitment of the homologous recombination-promoting protein complex TONSL-MMS22L to newly incorporated histones, as demonstrated recently (Saredi et al., 2016), and by concomitantly restraining the association of the 53BP1 anti-resection protein complex (this work). This dual mechanism enables localized repair pathway choice decisions on the basis of the absence or presence of

Europe PMC Funders Author Manuscripts

replicated template DNA sequences, and it ensures that the maximal strength of the 53BP1 anti-resection barrier is limited to pre-replicative chromatin.

Results

In light of the prominent role of 53BP1 to regulate repair pathway choice decisions (Chapman et al., 2012b; Ochs et al., 2016; Orthwein et al., 2015; Panier and Boulton, 2014; Pellegrino and Altmeyer, 2016; Schwertman et al., 2016), we set out to investigate the role of histone marks required for 53BP1 recruitment to damaged chromatin specifically as a function of cell cycle progression. To this end, we used quantitative image-based cytometry (QIBC), which allows cell cycle staging of asynchronously growing cell populations by automated high-content imaging (Ahuja et al., 2016; Altmeyer et al., 2013, 2015; Roukos et al., 2015; Toledo et al., 2013). This microscopy-based approach can be used to sensitively assess multiple cellular features and subcellular structures in individual cells and as a function of the cell cycle status independent of cell synchronization or other chemical or physical perturbations (Figure 1A). Using the total DAPI intensity per nucleus as a marker for DNA content, which doubles as cells progress from G1 to G2, we gated asynchronously growing U-2-OS cells into five subpopulation, roughly corresponding to G1, early S, mid S, late S, and G2 (Figure 1B). We then tested the levels of 53BP1's recognition mark H4K20me2 across the cell cycle. QIBC revealed a gradual decrease of H4K20me2 as cells progressed from G1 through S phase, with H4K20me2 levels being reduced to about 50% in late S phase and only going up again in a subpopulation of late G2 cells (Figures 1C and S1A). To validate these results using an independent approach, we synchronized cells with thymidine at the G1/S transition, released them from the cell cycle block for different time periods, and performed acid extraction of histones for western blot analysis (Figures S1B–S1D). These experiments confirmed the QIBC data and, consistent with previous reports (Alabert et al., 2015; Pesavento et al., 2008; Saredi et al., 2016), provide evidence that H4K20me2 in chromatin decreases as cells progress through S phase. In contrast, the levels of H4K16ac, another histone mark that affects 53BP1 accumulation in response to DNA damage (Jacquet et al., 2016; Tang et al., 2013), showed only very mild variation across the cell cycle (Figure S1E). Next, we quantified the amount of 53BP1 accumulation around DNA lesions together with H4K20me2 levels in unperturbed cells. Sub-nuclear 53BP1 accumulation under these conditions marks lesions originating from under-replicated DNA (e.g., at common fragile sites), which are processed during mitosis when sister chromatids separate (Harrigan et al., 2011; Lukas et al., 2011; Mankouri et al., 2013; Moreno et al., 2016). QIBC identified 53BP1 accumulation primarily in G1 and early S phase cells that contained high levels of H4K20me2 in unreplicated chromatin (Figure 1D). The nuclear 53BP1 bodies disappeared as cells progressed through S phase. Consistent with previous work (Chapman et al., 2012a), we observed that also after clastogen-inflicted DSB formation 53BP1 accumulation was most avid in G1 and early S phase cells, whereas its accumulation was markedly reduced in late S phase, when most of the genome had been replicated and H4K20me2 was lowest (Figures 1E and S2A–S2C). Co-staining experiments with EdU to directly mark S phase cells confirmed the association between 53BP1 and H4K20me2 (Figure 1F). Remarkably, both 53BP1 accumulation around DSBs and H4K20me2 were reproducibly reduced 2-fold when comparing late S to G1 cells (Figures

S2D and S2E). The specificity of the 53BP1 staining was confirmed by knockdown experiments (Figure S2F), a very similar trend was observed in cells stably expressing GFP-53BP1 (Figure S2G), and the compound UNC2170, a 53BP1 antagonist that obstructs its methyl-binding pocket (Perfetti et al., 2015), suppressed 53BP1 accumulation on damaged chromatin (Figure S3A). Moreover, blocking H4K20 di- and trimethylation by the SUV4-20 inhibitor A-196 (Bromberg et al., 2017) reduced H4K20me2 levels (Figure S3B), concomitantly increased H4K20me1 (Figure S3C), and impaired 53BP1 accumulation on damaged chromatin (Figures 1G and S3D), without affecting the upstream phosphorylation of H2AX (Figure S3E). Taken together, these results validate the specificity of our QIBC readouts, confirm the role of H4K20me2 in 53BP1 recruitment, and suggest that although 53BP1 marks IR-induced DNA lesions throughout interphase, its ability to do so is inversely correlated with the amount of replicated DNA and largely mirrors the availability of H4K20me2. To directly address whether 53BP1 accumulation in response to DSBs occurs more efficiently in pre- versus post-replicative chromatin, we combined a short EdU pulse with DSB induction by IR, staged cells according to their EdU and cyclin A levels (Figures 2A and 2B), and analyzed 53BP1 foci formation specifically in very early S phase cells (low DAPI/EdU/cyclin A with EdU marking all replicated areas of the genome). This revealed that 53BP1 foci poorly co-localize with EdU-marked replicated chromatin, supporting the notion that replicated chromatin is refractory to 53BP1 accumulation (Figure 2C). Similar analyses using confocal microscopy confirmed that in early S phase cells (marked by low DAPI/EdU) IR-induced 53BP1 accumulation showed a strong preference for non-replicated, EdU-negative areas of the genome (Figure 2D).

The cell cycle-dependent association between 53BP1 and H4K20me2 in unreplicated chromatin became even more apparent when we staged cells according to their H4K20me2 levels, quantified 53BP1 accumulation after different doses of irradiation, and normalized 53BP1 foci numbers to nuclear area to account for the increase in DNA content as cells progress through S phase (Figures 3A and 3B). These analyses recapitulated the previously described rate limitation of the RNF8/RNF168-driven 53BP1 response at higher doses of IR (Gudjonsson et al., 2012) and revealed a pronounced defect in marking DSBs in late S phase cells, when H4K20me2 levels are low. Additional experiments showed that this defect persisted at least from 45 min to 4 h after damage induction (Figure S4A), could be observed also when etoposide was used to induce breaks (Figure S4B), and was present in other cell lines tested (Figures S4C and S4D).

Interestingly, this gradually impaired recruitment appeared to be specific for 53BP1, because the formation of the upstream DNA damage signal γH2AX was largely independent of the amount of replicated DNA (Figures 3C and S5A). A prediction based on these findings is that the co-localization between 53BP1 and γH2AX should decrease as cells progress through the cell cycle. Indeed, we found that 53BP1 and γH2AX co-localized in G1 but that in mid and late S phase cells, an increasing number of γH2AX foci was not marked by 53BP1 accumulation (Figure 3D). Moreover, confocal imaging of EdU-labeled early S phase cells revealed that whereas most γH2AX foci co-localized with 53BP1, a small fraction did not and, different from 53BP1, was found in EdU-positive, replicated chromatin (Figure 3E). Thus, the discrimination between pre- and post-replicative chromatin occurs primarily at the level of 53BP1 and its detection of H4K20me2 rather than at a more apical level. In support

of this notion, the damage-induced RNF168-dependent ubiquitin conjugates upstream of 53BP1 accumulation (Gudjonsson et al., 2012; Thorslund et al., 2015) followed the trend observed for γH2AX (Figures 3F, S5B, and S5C), and also H2AK15 ubiquitylation did not show a drop in late S phase (Figure 3G) as measured by a specific antibody raised against K15-ubiquitylated H2A (Wang et al., 2016).

Conversely, and similar to 53BP1, the downstream effector and anti-resection regulator RIF1 also showed impaired focal accumulation in mid and late S phase (Figures 4A and S5D), and co-staining of irradiated cells for RIF1 and 53BP1 in conjunction with EdU labeling to mark S phase cells confirmed a strong positive correlation between RIF1 foci formation and 53BP1 accumulation throughout the cell cycle (Figure 4B), thus arguing that the differential recruitment of 53BP1 entails functional consequences for DNA end resection and the DSB repair pathway choice.

On the other hand, 53BP1's antagonist, the homologous recombination (HR) factor and tumor suppressor protein BRCA1, showed progressively increased accumulation around IR-induced DSBs as cells progressed through S phase, consistent with increased HDR in replicated areas of the genome (Figures 4C and S5E). A very similar trend was observed when we directly measured DNA end resection as a hallmark of HDR: native BrdU assays showed that resection scaled with the amount of replicated DNA and was inversely correlated with H4K20me2 levels; that is, the highest degree of DNA end resection was observed in cells with lowest H4K20me2 levels in late S phase, despite FK2 and H2AK15ub foci being up in late S phase under these conditions (Figures 4D, S5F, and S5G).

Taken together, these data reveal an intricate link between H4K20me2 levels in chromatin and DSB repair pathway choice: the replication-coupled dilution of H4K20me2 in post-replicative chromatin represents an inbuilt mechanism to reinforce 53BP1's engagement in pre-replicative chromatin, which is needed to restrict DNA end resection and promote repair by NHEJ, and at the same time lowers the affinity of 53BP1 to DSB-surrounding chromatin in replicated regions of the genome in order to facilitate repair by HDR.

BRCA1 was previously shown to displace 53BP1 from chromatin in the vicinity of DSBs, thus countering the resection barrier and promoting HDR in S phase (Chapman et al., 2012a). Accordingly, BRCA1's function to displace 53BP1 might synergize with 53BP1's reduced affinity to DSBs in post-replicative chromatin containing low H4K20me2 levels. Indeed, and consistent with previous work (Chapman et al., 2012a), when we depleted BRCA1 by small interfering RNA (siRNA), the drop in 53BP1 focal accumulation in late S phase cells after IR was completely abolished, despite the fact that H4K20me2 patterns remained largely unchanged (Figure 5A). Importantly, however, inhibition of H4K20 di- and trimethylation by A-196 partially reduced 53BP1 recruitment even in BRCA1-depleted cells (Figure 5B). We therefore conclude that the replication-coupled dilution of H4K20me2 functionally cooperates with BRCA1 by lowering the threshold to displace 53BP1 from replicated chromatin and thereby facilitates HDR.

The H4K20-targeting methyltransferase SET8 acts upstream of SUV4-20 (Beck et al., 2012) and is likely the rate-limiting factor for restoring parental H4K20me2 levels in replicated

chromatin. Interestingly, SET8 is degraded specifically during the S phase of the cell cycle and in a PCNA-dependent manner (Beck et al., 2012; Jørgensen et al., 2011, 2013; Oda et al., 2010), raising the possibility that maintaining low levels of SET8 during S phase progression prevents premature restoration of H4K20 methylation patterns in post-replicative chromatin. We thus overexpressed SET8 in cells, reasoning that this should elevate the levels of H4K20me2, particularly in post-replicative chromatin, given that H4K20me2 is highly abundant and close to saturation in pre-replicative chromatin (Pesavento et al., 2008). We expressed HA-FLAG-tagged wild-type SET8, a PIP2 deletion mutant (SET8 *) that is resistant to S phase-specific PCNA-dependent degradation (Jørgensen et al., 2011), and a mutant that is catalytically inactive (SET8 †). Using QIBC, we discriminated cells with ectopic SET8 expression on the basis of a positive HA signal from HA-negative cells (Figure S5H) and monitored H4K20me2 and 53BP1 accumulation. Although expression of wild-type SET8 only mildly elevated H4K20me2 levels in late S phase, most likely because it was not inert against S phase-specific degradation (Figure S5H), the non-degradable version of SET8 clearly enhanced H4K20me2 levels in late S phase (Figure 5C, left, and Figure S5H). Remarkably, the non-degradable SET8 and, to a lesser extent, also overexpression of wild-type SET8 rescued 53BP1 accumulation in late S phase, while the catalytically inactive mutant could neither level the H4K20me2 pattern nor significantly alter 53BP1 (Figure 5C). Consistent with elevated 53BP1 accumulation on damaged chromatin upon SET8 * overexpression, HA-positive cells showed markedly reduced accumulation of BRCA1 and RAD51 in response to IR (Figures 5D and 5E). To further corroborate these data, we depleted two ubiquitin ligase complex components, CDT2 and beta-TRCP, which cooperate to mediate PCNA-dependent SET8 degradation (Jørgensen et al., 2011; Oda et al., 2010; Wang et al., 2015). Consistent with the SET8 overexpression data, depletion of CDT2/beta-TRCP mitigated the drop in H4K20me2 levels in mid/late S phase (Figure 5F) and partially rescued the accumulation of 53BP1 in post-replicative chromatin (Figure 5G).

Collectively, our findings unravel a role for H4K20me2 in modulating the 53BP1 response to DSBs throughout S phase, thereby guiding the DSB repair pathway choice in a locus-specific manner as a function of pre- versus post-replicative chromatin. This provides experimental support for the recently proposed post-replicative chromatin marking model (Hustedt and Durocher, 2016) and extends previous work on the HR-promoting role of newly incorporated histones (Saredi et al., 2016) to an additional role as NHEJ antagonists by restraining 53BP1 accumulation (Figure 6). Coupling the balance between HR and NHEJ to histone marks, whose abundance discriminates pre- from post-replicative chromatin thus represents an elegant inbuilt dual mechanism to choose the appropriate DSB repair pathway dependent on the absence or availability of a homologous template strand.

Discussion

Cells regulate DSB repair pathways both globally (e.g., by pannuclear signals) and locally (e.g., as a function of the chromatin environment or the transcription status). For instance, by virtue of mitotic kinases, 53BP1 is globally prevented from binding to broken chromosomes during mitosis in order to prevent aberrant telomere fusions (Orthwein et al., 2014). Similarly, HR is suppressed in G1 by a cell cycle-regulated ubiquitylation circuit, which

prevents formation of the BRCA1-PALB2-BRCA2 complex prior to S phase entry (Orthwein et al., 2015). Further, as cells progress into S phase, the ability to form functional BRCA1-PALB2-BRCA2 complexes synergizes with the CDK activity-mediated globally enhanced processivity of the resection machinery (Huertas et al., 2008; Ira et al., 2004) as well as with the nuclear export of the resection antagonist HELB (Tkáč et al., 2016). Although such global regulation can efficiently prevent untimely engagement of repair pathways and help to set the right conditions for appropriate repair pathway decisions, it is insufficient to guide the choice between NHEJ and HDR as cells progress through S phase and when unreplicated and replicated areas of the genome co-exist within the same nucleus. Throughout S phase, DSB repair must therefore be regulated also locally and dependent on the availability of replicated DNA sequences as templates for repair. The chromatin makeup in front of and behind the replication fork may constitute a means to guide repair pathway choices (Hustedt and Durocher, 2016). Indeed, it was recently shown that the HR-promoting TONSL-MMS22L complex is recruited to newly incorporated histones in post-replicative chromatin by recognizing unmethylated H4K20 tails (Saredi et al., 2016). Our data complement and further extend these findings by showing that post-replicative chromatin not only supports recruitment of HR factors, but at the same time is refractory to 53BP1 accumulation.

Consistent with our findings on cell cycle resolved DNA damage-induced chromatin modifications, previous nascent chromatin capture (NCC) experiments coupled to SILAC-based mass spectrometry to analyze histones and their marks on parental histones and in newly replicated DNA provided evidence that di- and trimethylation marks are diluted 2-fold upon replication, whereas the histone variant H2AX is quickly incorporated into newly replicated DNA (Alabert et al., 2014, 2015). Taken together, this suggests that whereas the apical, H2AX-based responses to DSBs can work efficiently in pre- and post-replicative chromatin, the downstream and repair pathway determining response at the level of 53BP1 and its effectors works more efficiently in pre- versus post-replicative chromatin. From an evolutionary perspective 53BP1 may have evolved as a bivalent histone reader in order to be able to couple the sensing of a damage-induced chromatin signal (H2AK15ub, generated de novo in the vicinity of DSBs through cooperative action of the ATM/MDC1/RNF8/RNF168 signaling cascade) with the sensing of unreplicated chromatin (marked by high H4K20me2 levels). In this way, cells ensure that the 53BP1-mediated constraint to DNA end resection is most efficient in genomic areas, which have yet to be replicated, and in which resection would lead to loss of genetic information. We noticed that 53BP1 accumulation occurs again in a subpopulation of late G2 cells, when H4K20me2 levels are restored, and it is interesting to speculate that NHEJ might be particularly suppressed in post-replicative chromatin during S phase progression, when replication intermediates bear a high risk for NHEJ-mediated chromosome fusions, and is enabled again in late G2 when the vast majority of replication intermediates has been resolved.

Our model is compatible with a recently described function of 53BP1 to restrain resection throughout S phase in order to favor gene conversion over single strand annealing (Ochs et al., 2016). In fact, compared with pre-replicative chromatin, nascent chromatin with low levels of H4K20me2 might be exquisitely prone to undergo mutagenic single strand annealing upon breakage under conditions when 53BP1 becomes limiting. Although

previous work (Saredi et al., 2016) and our data indicate that DSB repair pathway choice is inherently linked to replication-coupled changes in the chromatin state, our results neither exclude that H4K20me2 is locally modulated in response to DNA damage to provide an additional layer of regulation, nor that additional genomic features and chromatin states impact the repair pathway choice during S phase progression.

An important ramification of our model relates to current gene targeting approaches, which are generally limited by the efficiency of HDR. In G1 cells, for instance, HDR is suppressed by a cell cycle-regulated ubiquitylation circuit, which prevents formation of the BRCA1-PALB2-BRCA2 HDR complex and thereby limits gene targeting (Orthwein et al., 2015). Our data suggest that also during S phase, constraints exist for HDR, one of them being the histone methylation status of H4K20. Because H4K20 methylation is tightly coupled to DNA replication, cell-type-specific differences in replication timing and the corresponding maturation of epigenetic marks may emerge as relevant factors for gene targeting approaches and their therapeutic application.

Experimental Procedures

Cell Culture, DNA Damage Treatments, and Nucleoside Analogs

Human U-2-OS, HeLa, and hTERT-RPE1 cells as well as U-2-OS cells stably expressing GFP-53BP1 (kind gift of Jiri Lukas) were grown under standard cell culture conditions (humidified atmosphere, 5% CO_2) in DMEM containing 10% fetal bovine serum (GIBCO) and penicillin-streptomycin antibiotics. All cell lines were routinely tested for potential mycoplasma contamination and scored negatively. X-ray irradiation (0.5–5 Gy) of cells was performed with a XYLON.SMART 160E/1.5 device, a RS-2000 Rad Source Irradiator, and a Faxitron Cabinet X-ray System Model RX-650. Etoposide (Selleckchem) was used at a final concentration of 5 μM, and cells were treated for 1–4 hr as indicated. Thymidine (Sigma) and Nocodazole (Sigma) were used at final concentrations of 2 mM and 50 ng/ml, respectively. BrdU (5-bromo-2-deoxyuridine; Sigma) was used at a final concentration of 10 μM, and cells were allowed to incorporate BrdU for 24 hr. For pulsed EdU (5-ethynyl-2′-desoxyuridine; Thermo Fisher Scientific) incorporation, cells were incubated for 20 min in medium containing 10 μM EdU. The Click-iT EdU Alexa Fluor 488 Imaging Kit (Thermo Fisher Scientific) was used for EdU detection. The SUV4-20 inhibitor A-196 (Sigma) was used at a final concentration of 1 μM for 24–72 hr, and UNC2170 (Sigma) was used at a final concentration of 300 μM for 4 hr.

Plasmid and siRNA Transfections

Plasmid transfections were performed with polyethylenimine (PEI) according to standard procedures using a PEI/DNA ratio of 2:1. The following plasmids were used for transfections: pCMV-HA-FLAG-SET8 wild-type, pCMV-HA-FLAG-SET8 PIP2 mutant (LTDFY), pCMV-HA-FLAG-SET8 methyltransferase dead (NH/AA) (Jørgensen et al., 2011). Cells were treated and fixed 24 hr after transfection. Duplex siRNA transfections were performed for 72 hr with Ambion Silencer Select siRNAs using Lipofectamine RNAiMAX (Thermo Fisher Scientific). The following Silencer Select siRNAs were used at a final concentration of 25 nM: 53BP1 (s14313), BRCA1 (s459), CDT2 (s226739), bTRCP

(s17109), and RNF168 (s46600). Negative control (4390843) from Ambion was used as a non-targeting control and is abbreviated as “siCon.”

Cell Synchronization and Histone Extraction

For cell synchronization and release experiments, exponentially growing U-2-OS cells were incubated with 2 mM thymidine for 20 hr and subsequently washed and cultured in fresh medium. For cell synchronization in G2/M exponentially growing U-2-OS cells were incubated with nocodazole (50 ng/ml) for 14 hr. For acid extraction of histones, cell pellets were resuspended in Triton Extraction Buffer (TEB: PBS containing 0.5% Triton X-100 [v/v], 2 mM PMSF, 0.02% [w/v] NaN_3) at a cell density of 10^7 cells/mL and lysed on ice for 10 min. Cells were centrifuged at 6,500 × *g* for 10 min at 4°C and then washed with TEB at a cell density of 2×10^7 cells/ml. Cell pellets were resuspended in 0.2 N HCl at a density of 4×10^7 nuclei per ml and extracted over night at 4°C. Samples were centrifuged at 6,500 × *g* for 10 min at 4°C and the supernatants neutralized with 20% 1 M NaOH. Protein amounts were quantified using the standard Bradford method.

Immunochemical Methods

Proteins were resolved by SDS-PAGE and transferred onto polyvinylidene fluoride (PVDF) membranes. Membranes were blocked with PBS-Tween 20 (0.01%) containing 5% milk powder for 1 hr at room temperature. Primary antibodies in blocking solution were applied over night at 4°C. The following primary antibodies were used for western blot analysis: H4K20me2 (rabbit, Abcam ab9052, 1:500), H4 (rabbit, Abcam ab10158, 1:5,000), H3 (rabbit, Abcam ab1791, 1:20,000). Secondary horseradish peroxidase-coupled antibodies (Vector Labs and Thermo Fisher Scientific) were applied for 1 hr at room temperature in PBS-Tween 20 (0.01%) containing 1% milk powder prior to detection by ECL-based chemiluminescence.

Immunostaining

Cells were grown on sterile 12 mm glass coverslips, fixed in 3% formaldehyde in PBS for 12 min at room temperature, washed once in PBS, permeabilized for 5 min at room temperature in 0.2% Triton X-100 (Sigma-Aldrich) in PBS, and washed twice in PBS. For native BrdU stainings, cells were pre-extracted in 0.2% Triton X-100 in PBS for 2 min on ice prior to formaldehyde fixation. All primary antibodies (see below for specifications) and secondary antibodies (Alexa fluorophores, Life Technologies) were diluted in filtered DMEM containing 10% FBS and 0.02% sodium azide. Antibody incubations were performed for 1–2 hr at room temperature. Following antibody incubations, coverslips were washed once with PBS and incubated for 2 min with PBS containing DAPI (0.5 μg/mL) at room temperature to stain DNA. Following three washing steps in PBS, coverslips were briefly washed with distilled water and mounted on 5 μL Mowiol-based mounting media (Mowiol 4.88 [Calbiochem]/glycerol/Tris). The following primary antibodies were used for immunostaining: H2AX Phospho S139 (mouse, Biolegend 613401, 1:1,000), 53BP1 (rabbit, Santa Cruz sc-22760, 1:500), 53BP1 (mouse, Upstate MAB3802, 1:1,000), H4K20me2 (rabbit, Abcam ab9052, 1:100), H4K20me1 (rabbit, Abcam ab9051, 1:1,000), H4K16ac (rabbit, Abcam ab109463, 1:100), H2AK15ub (mouse, 1:300, kind gift of Zhiguo Zhang), RIF1 (rabbit, Bethyl A300-569A, 1:1,000), BRCA1 (mouse, Santa Cruz sc-6954, 1:100),

RAD51 (rabbit, Bioacademia 70-002, 1:1,000), FK2 (mouse, Enzo Life Sciences BML-PW8810-0500, 1:1,000), Cyclin A (mouse, Abcam ab 16726, 1:100), BrdU (mouse, Becton Dickinson 347580, 1:100), HA (mouse, BioLegend 901501, 1:250), HA (rabbit, Abcam ab9110, 1:1,000).

QIBC and Confocal Microscopy

Automated multichannel wide-field microscopy for QIBC was performed as described previously (Altmeyer et al., 2013; Toledo et al., 2013; Duda et al., 2016; Ochs et al., 2016) on an Olympus ScanR Screening System equipped with an inverted motorized Olympus IX83 microscope, a motorized stage, IR-laser hardware autofocus, a fast emission filter wheel with single-band emission filters, and a 12-bit digital monochrome Hamamatsu ORCA-FLASH 4.0 V2 sCMOS camera (dynamic range 4,000:1, 2,048 × 2,948 pixel of size 6.5 × 6.5 μm, 12-bit dynamics). For each condition, image information of large cohorts of cells (typically at least 500 cells for the UPLSAPO 40× objective [NA 0.9], at least 2,000 cells for the UPLSAPO 20× objective [NA 0.75], and at least 5,000 cells for the UPLSAPO 10× [NA 0.4] and UPLSAPO 4× [NA 0.16] objectives was acquired under non-saturating conditions. Identical settings were applied to all samples within one experiment. Images were analyzed with the inbuilt Olympus ScanR Image Analysis Software Version 2.5.1, a dynamic background correction was applied, nuclei segmentation was performed using an integrated intensity-based object detection module using the DAPI signal, and foci segmentation was performed using an integrated spot-detection module. Fluorescence intensities were quantified and are depicted as arbitrary units. Color-coded scatterplots of asynchronous cell populations were generated with Spotfire data visualization software (TIBCO). Within one experiment, similar cell numbers were compared for the different conditions. To visualize discrete data in scatterplots (e.g., foci numbers), mild jittering (random displacement of data points along the discrete data axes) was applied in order to demerge overlapping data points. Representative scatterplots and quantifications of independent experiments, typically containing several thousand cells each, are shown. Confocal microscopy was performed on a Leica SP8 laser scanning microscope equipped with solid-state diode lasers for 405 nm (50 mW), 488 nm (20 mW), 552 nm (20 mW), and 638 nm (30 mW) using an HCX PL APO CS2 63× immersion oil objective (NA 1.4).

Statistical Methods

Averages and SDs from $n \geq 3$ samples were calculated, and averages were compared using unpaired t tests. p values < 0.05 were considered to indicate statistical significance.

Supplementary Material

Refer to Web version on PubMed Central for supplementary material.

Acknowledgments

We would like to thank Claus Sørensen for kindly providing the SET8 plasmids, Jiri Lukas for the generous gift of the GFP-53BP1 cell line, Zhiguo Zhang for the H2AK15ub antibody, and Lorenza Penengo for sharing IF reagents. We are grateful to Jiri Lukas, Claus Sørensen, Kai Neelsen, and Anja Groth for helpful discussions and comments on the manuscript. We acknowledge the Center for Microscopy and Image Analysis at the University of Zurich, in particular Urs Ziegler and José María Mateos Melero, for excellent microscopy support. Research in the lab of

Matthias Altmeyer is supported by the Swiss National Science Foundation (SNSF Professorship Grant PP00P3_150690), the European Research Council (Horizon 2020 ERC-2016-STG 714326 DiVineGenoMe), and the University of Zurich Association Research Talent Development Fund. S.P. and F.T. are members of the Molecular Life Sciences Program of the Life Science Zurich Graduate School. J.M. is supported by the Gobierno Vasco Programa Posdoctoral de Perfeccionamiento de Personal Investigador Doctor. F.T. is supported by a fellowship of the UZH Forschungskredit Candoc Program.

References

Acs K, Luijsterburg MS, Ackermann L, Salomons FA, Hoppe T, Dantuma NP. The AAA-ATPase VCP/p97 promotes 53BP1 recruitment by removing L3MBTL1 from DNA double-strand breaks. Nat Struct Mol Biol. 2011; 18:1345–1350. [PubMed: 22120668]

Ahuja AK, Jodkowska K, Teloni F, Bizard AH, Zellweger R, Herrador R, Ortega S, Hickson ID, Altmeyer M, Mendez J, Lopes M. A short G1 phase imposes constitutive replication stress and fork remodelling in mouse embryonic stem cells. Nat Commun. 2016; 7:10660. [PubMed: 26876348]

Alabert C, Bukowski-Wills JC, Lee SB, Kustatscher G, Nakamura K, de Lima Alves F, Menard P, Mejlvang J, Rappsilber J, Groth A. Nascent chromatin capture proteomics determines chromatin dynamics during DNA replication and identifies unknown fork components. Nat Cell Biol. 2014; 16:281–293. [PubMed: 24561620]

Alabert C, Barth TK, Reverón-Gómez N, Sidoli S, Schmidt A, Jensen ON, Imhof A, Groth A. Two distinct modes for propagation of histone PTMs across the cell cycle. Genes Dev. 2015; 29:585–590. [PubMed: 25792596]

Altmeyer M, Lukas J. Guarding against collateral damage during chromatin transactions. Cell. 2013; 153:1431–1434. [PubMed: 23791174]

Altmeyer M, Toledo L, Gudjonsson T, Grøfte M, Rask MB, Lukas C, Akimov V, Blagoev B, Bartek J, Lukas J. The chromatin scaffold protein SAFB1 renders chromatin permissive for DNA damage signaling. Mol Cell. 2013; 52:206–220. [PubMed: 24055346]

Altmeyer M, Neelsen KJ, Teloni F, Pozdnyakova I, Pellegrino S, Grøfte M, Rask MB, Streicher W, Jungmichel S, Nielsen ML, Lukas J. Liquid demixing of intrinsically disordered proteins is seeded by poly(ADP-ribose). Nat Commun. 2015; 6:8088. [PubMed: 26286827]

Beck DB, Oda H, Shen SS, Reinberg D. PR-Set7 and H4K20me1: at the crossroads of genome integrity, cell cycle, chromosome condensation, and transcription. Genes Dev. 2012; 26:325–337. [PubMed: 22345514]

Botuyan MV, Lee J, Ward IM, Kim JE, Thompson JR, Chen J, Mer G. Structural basis for the methylation state-specific recognition of histone H4-K20 by 53BP1 and Crb2 in DNA repair. Cell. 2006; 127:1361–1373. [PubMed: 17190600]

Bromberg KD, Mitchell TR, Upadhyay AK, Jakob CG, Jhala MA, Comess KM, Lasko LM, Li C, Tuzon CT, Dai Y, et al. The SUV4-20 inhibitor A-196 verifies a role for epigenetics in genomic integrity. Nat Chem Biol. 2017; 13:317–324. [PubMed: 28114273]

Ceccaldi R, Rondinelli B, D'Andrea AD. Repair pathway choices and consequences at the double-strand break. Trends Cell Biol. 2016; 26:52–64. [PubMed: 26437586]

Chapman JR, Sossick AJ, Boulton SJ, Jackson SP. BRCA1-associated exclusion of 53BP1 from DNA damage sites underlies temporal control of DNA repair. J Cell Sci. 2012a; 125:3529–3534. [PubMed: 22553214]

Chapman JR, Taylor MRG, Boulton SJ. Playing the end game: DNA double-strand break repair pathway choice. Mol Cell. 2012b; 47:497–510. [PubMed: 22920291]

Duda H, Arter M, Gloggnitzer J, Teloni F, Wild P, Blanco MG, Altmeyer M, Matos J. A mechanism for controlled breakage of under-replicated chromosomes during mitosis. Dev Cell. 2016; 39:740–755. [PubMed: 27997828]

Dulev S, Tkach J, Lin S, Batada NN. SET8 methyltransferase activity during the DNA double-strand break response is required for recruitment of 53BP1. EMBO Rep. 2014; 15:1163–1174. [PubMed: 25252681]

Fradet-Turcotte A, Canny MD, Escribano-Díaz C, Orthwein A, Leung CCY, Huang H, Landry MC, Kitevski-LeBlanc J, Noordermeer SM, Sicheri F, Durocher D. 53BP1 is a reader of the DNA-damage-induced H2A Lys 15 ubiquitin mark. Nature. 2013; 499:50–54. [PubMed: 23760478]

Europe PMC Funders Author Manuscripts

Gatti M, Pinato S, Maspero E, Soffientini P, Polo S, Penengo L. A novel ubiquitin mark at the N-terminal tail of histone H2As targeted by RNF168 ubiquitin ligase. Cell Cycle. 2012; 11:2538–2544. [PubMed: 22713238]

Greeson NT, Sengupta R, Arida AR, Jenuwein T, Sanders SL. Di-methyl H4 lysine 20 targets the checkpoint protein Crb2 to sites of DNA damage. J Biol Chem. 2008; 283:33168–33174. [PubMed: 18826944]

Gudjonsson T, Altmeyer M, Savic V, Toledo L, Dinant C, Grøfte M, Bartkova J, Poulsen M, Oka Y, Bekker-Jensen S, et al. TRIP12 and UBR5 suppress spreading of chromatin ubiquitylation at damaged chromosomes. Cell. 2012; 150:697–709. [PubMed: 22884692]

Harrigan JA, Belotserkovskaya R, Coates J, Dimitrova DS, Polo SE, Bradshaw CR, Fraser P, Jackson SP. Replication stress induces 53BP1-containing OPT domains in G1 cells. J Cell Biol. 2011; 193:97–108. [PubMed: 21444690]

Huertas P, Cortés-Ledesma F, Sartori AA, Aguilera A, Jackson SP. CDK targets Sae2 to control DNA-end resection and homologous recombination. Nature. 2008; 455:689–692. [PubMed: 18716619]

Hustedt N, Durocher D. The control of DNA repair by the cell cycle. Nat Cell Biol. 2016; 19:1–9. [PubMed: 28008184]

Ira G, Pellicioli A, Balijja A, Wang X, Fiorani S, Carotenuto W, Liberi G, Bressan D, Wan L, Hollingsworth NM, et al. DNA end resection, homologous recombination and DNA damage checkpoint activation require CDK1. Nature. 2004; 431:1011–1017. [PubMed: 15496928]

Jacquet K, Fradet-Turcotte A, Avvakumov N, Lambert JP, Roques C, Pandita RK, Paquet E, Herst P, Gingras AC, Pandita TK, et al. The TIP60 complex regulates bivalent chromatin recognition by 53BP1 through direct H4K20me binding and H2AK15 acetylation. Mol Cell. 2016; 62:409–421. [PubMed: 27153538]

Jørgensen S, Eskildsen M, Fugger K, Hansen L, Larsen MSY, Kousholt AN, Syljuåsen RG, Trelle MB, Jensen ON, Helin K, Sørensen CS. SET8 is degraded via PCNA-coupled CRL4(CDT2) ubiquitylation in S phase and after UV irradiation. J Cell Biol. 2011; 192:43–54. [PubMed: 21220508]

Jørgensen S, Schotta G, Sørensen CS. Histone H4 lysine 20 methylation: key player in epigenetic regulation of genomic integrity. Nucleic Acids Res. 2013; 41:2797–2806. [PubMed: 23345616]

Lukas C, Savic V, Bekker-Jensen S, Doil C, Neumann B, Pedersen RS, Grøfte M, Chan KL, Hickson ID, Bartek J, Lukas J. 53BP1 nuclear bodies form around DNA lesions generated by mitotic transmission of chromosomes under replication stress. Nat Cell Biol. 2011; 13:243–253. [PubMed: 21317883]

Mallette FA, Mattiroli F, Cui G, Young LC, Hendzel MJ, Mer G, Sixma TK, Richard S. RNF8- and RNF168-dependent degradation of KDM4A/JMJD2A triggers 53BP1 recruitment to DNA damage sites. EMBO J. 2012; 31:1865–1878. [PubMed: 22373579]

Mankouri HW, Huttner D, Hickson ID. How unfinished business from S-phase affects mitosis and beyond. EMBO J. 2013; 32:2661–2671. [PubMed: 24065128]

Mattiroli F, Vissers JHA, van Dijk WJ, Ikpa P, Citterio E, Vermeulen W, Marteijn JA, Sixma TK. RNF168 ubiquitinates K13-15 on H2A/H2AX to drive DNA damage signaling. Cell. 2012; 150:1182–1195. [PubMed: 22980979]

Moreno A, Carrington JT, Albergante L, Al Mamun M, Haagensen EJ, Komseli ES, Gorgoulis VG, Newman TJ, Blow JJ. Unreplicated DNA remaining from unperturbed S phases passes through mitosis for resolution in daughter cells. Proc Natl Acad Sci U S A. 2016; 113:E5757–E5764. [PubMed: 27516545]

Ochs F, Somyajit K, Altmeyer M, Rask MB, Lukas J, Lukas C. 53BP1 fosters fidelity of homology-directed DNA repair. Nat Struct Mol Biol. 2016; 23:714–721. [PubMed: 27348077]

Oda H, Hübner MR, Beck DB, Vermeulen M, Hurwitz J, Spector DL, Reinberg D. Regulation of the histone H4 monomethylase PR-Set7 by CRL4(Cdt2)-mediated PCNA-dependent degradation during DNA damage. Mol Cell. 2010; 40:364–376. [PubMed: 21035370]

Orthwein A, Fradet-Turcotte A, Noordermeer SM, Canny MD, Brun CM, Strecker J, Escribano-Diaz C, Durocher D. Mitosis inhibits DNA double-strand break repair to guard against telomere fusions. Science. 2014; 344:189–193. [PubMed: 24652939]

Orthwein A, Noordermeer SM, Wilson MD, Landry S, Enchev RI, Sherker A, Munro M, Pinder J, Salsman J, Dellaire G, et al. A mechanism for the suppression of homologous recombination in G1 cells. Nature. 2015; 528:422–426. [PubMed: 26649820]

Panier S, Boulton SJ. Double-strand break repair: 53BP1 comes into focus. Nat Rev Mol Cell Biol. 2014; 15:7–18. [PubMed: 24326623]

Pei H, Zhang L, Luo K, Qin Y, Chesi M, Fei F, Bergsagel PL, Wang L, You Z, Lou Z. MMSET regulates histone H4K20 methylation and 53BP1 accumulation at DNA damage sites. Nature. 2011; 470:124–128. [PubMed: 21293379]

Pellegrino S, Altmeyer M. Interplay between ubiquitin, SUMO, and poly(ADP-ribose) in the cellular response to genotoxic stress. Front Genet. 2016; 7:63. [PubMed: 27148359]

Perfetti MT, Baughman BM, Dickson BM, Mu Y, Cui G, Mader P, Dong A, Norris JL, Rothbart SB, Strahl BD, et al. Identification of a fragment-like small molecule ligand for the methyl-lysine binding protein, 53BP1. ACS Chem Biol. 2015; 10:1072–1081. [PubMed: 25590533]

Pesavento JJ, Yang H, Kelleher NL, Mizzen CA. Certain and progressive methylation of histone H4 at lysine 20 during the cell cycle. Mol Cell Biol. 2008; 28:468–486. [PubMed: 17967882]

Roukos V, Pegoraro G, Voss TC, Misteli T. Cell cycle staging of individual cells by fluorescence microscopy. Nat Protoc. 2015; 10:334–348. [PubMed: 25633629]

Saredi G, Huang H, Hammond CM, Alabert C, Bekker-Jensen S, Forne I, Reverón-Gómez N, Foster BM, Mlejnkova L, Bartke T, et al. H4K20me0 marks post-replicative chromatin and recruits the TONSL–MMS22L DNA repair complex. Nature. 2016; 534:714–718. [PubMed: 27338793]

Schwertman P, Bekker-Jensen S, Mailand N. Regulation of DNA double-strand break repair by ubiquitin and ubiquitin-like modifiers. Nat Rev Mol Cell Biol. 2016; 17:379–394. [PubMed: 27211488]

Tang J, Cho NW, Cui G, Manion EM, Shanbhag NM, Botuyan MV, Mer G, Greenberg RA. Acetylation limits 53BP1 association with damaged chromatin to promote homologous recombination. Nat Struct Mol Biol. 2013; 20:317–325. [PubMed: 23377543]

Thorslund T, Ripplinger A, Hoffmann S, Wild T, Uckelmann M, Villumsen B, Narita T, Sixma TK, Choudhary C, Bekker-Jensen S, Mailand N. Histone H1 couples initiation and amplification of ubiquitin signalling after DNA damage. Nature. 2015; 527:389–393. [PubMed: 26503038]

Tkáč J, Xu G, Adhikary H, Young JTF, Gallo D, Escribano-Díaz C, Krietsch J, Orthwein A, Munro M, Sol W, et al. HELB is a feedback inhibitor of DNA end resection. Mol Cell. 2016; 61:405–418. [PubMed: 26774285]

Toledo LI, Altmeyer M, Rask MB, Lukas C, Larsen DH, Povlsen LK, Bekker-Jensen S, Mailand N, Bartek J, Lukas J. ATR prohibits replication catastrophe by preventing global exhaustion of RPA. Cell. 2013; 155:1088–1103. [PubMed: 24267891]

Tuzon CT, Spektor T, Kong X, Congdon LM, Wu S, Schotta G, Yokomori K, Rice JC. Concerted activities of distinct H4K20 methyltransferases at DNA double-strand breaks regulate 53BP1 nucleation and NHEJ-directed repair. Cell Rep. 2014; 8:430–438. [PubMed: 25001286]

Wang Z, Dai X, Zhong J, Inuzuka H, Wan L, Li X, Wang L, Ye X, Sun L, Gao D, et al. SCF(β-TRCP) promotes cell growth by targeting PR-Set7/Set8 for degradation. Nat Commun. 2015; 6:10185. [PubMed: 26666832]

Wang Z, Zhang H, Liu J, Cheruiyot A, Lee JH, Ordog T, Lou Z, You Z, Zhang Z. USP51 deubiquitylates H2AK13,15ub and regulates DNA damage response. Genes Dev. 2016; 30:946–959. [PubMed: 27083998]

Wilson MD, Benlekbir S, Fradet-Turcotte A, Sherker A, Julien JP, McEwan A, Noordermeer SM, Sicheri F, Rubinstein JL, Durocher D. The structural basis of modified nucleosome recognition by 53BP1. Nature. 2016; 536:100–103. [PubMed: 27462807]

Zimmermann M, de Lange T. 53BP1: pro choice in DNA repair. Trends Cell Biol. 2014; 24:108–117. [PubMed: 24094932]

Europe PMC Funders Author Manuscripts

Highlights

- The genome caretaker 53BP1 preferentially marks DSBs in pre-replicative chromatin
- Replication-coupled dilution of H4K20me2 restrains 53BP1 function
- DSB repair pathway choice is linked to replication status of broken genomic loci
- Premature chromatin maturation shifts the balance from HDR to NHEJ activities

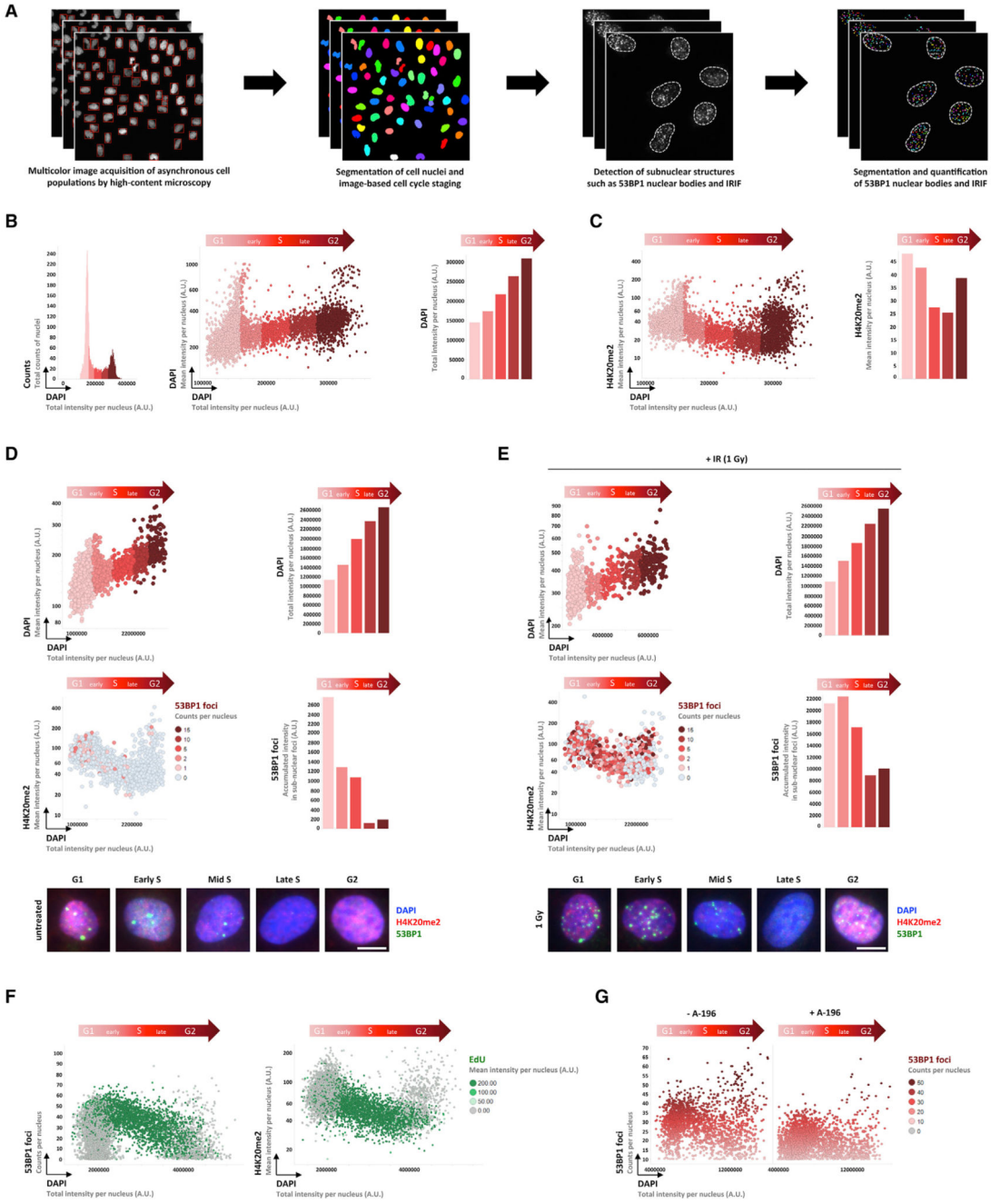

Figure 1. 53BP1 Marks DSBs Preferentially in Pre-replicative Chromatin with High Levels of H4K20me2

(A) Experimental setup for quantitative image-based cytometry (QIBC), which allows us to assess cellular features (e.g., ionizing radiation-induced foci [IRIF]) in individual cells of large cell populations as a function of the cell cycle status.

(B) QIBC for cell cycle staging of asynchronous cell populations. DAPI-based 1D and 2D cell cycle profiles of U-2-OS cells are shown. Cells were gated into five sub-populations with increasing DNA content from G1 to G2.

(C) H4K20me2 levels across the cell cycle based on QIBC.

Europe PMC Funders Author Manuscripts

(D) Asynchronously growing unperturbed U-2-OS cells were stained for H4K20me2 and 53BP1. Accumulated intensities in sub-nuclear 53BP1 bodies are shown as a function of cell cycle progression and H4K20me2 levels. Representative cells are shown below.
(E) Cells were fixed 45 min after 1 Gy of IR and stained for H4K20me2 and 53BP1. Accumulated 53BP1 intensities in sub-nuclear foci are shown as a function of cell cycle progression and H4K20me2 levels. Representative cells are shown below.
(F) Cells were pulsed with EdU for 20 min, irradiated as in (E), and stained for EdU, 53BP1, and H4K20me2. 53BP1 foci counts and H4K20me2 levels are shown as a function of cell cycle progression.
(G) Cells were treated for 48 hr with 1 μM SUV4-20 inhibitor A-196, irradiated with 1 Gy, fixed after 45 min, and stained for 53BP1.
Color codes as defined in the figure panels. The scale bars represent 10 μm. See also Figures S1–S3.

Europe PMC Funders Author Manuscripts

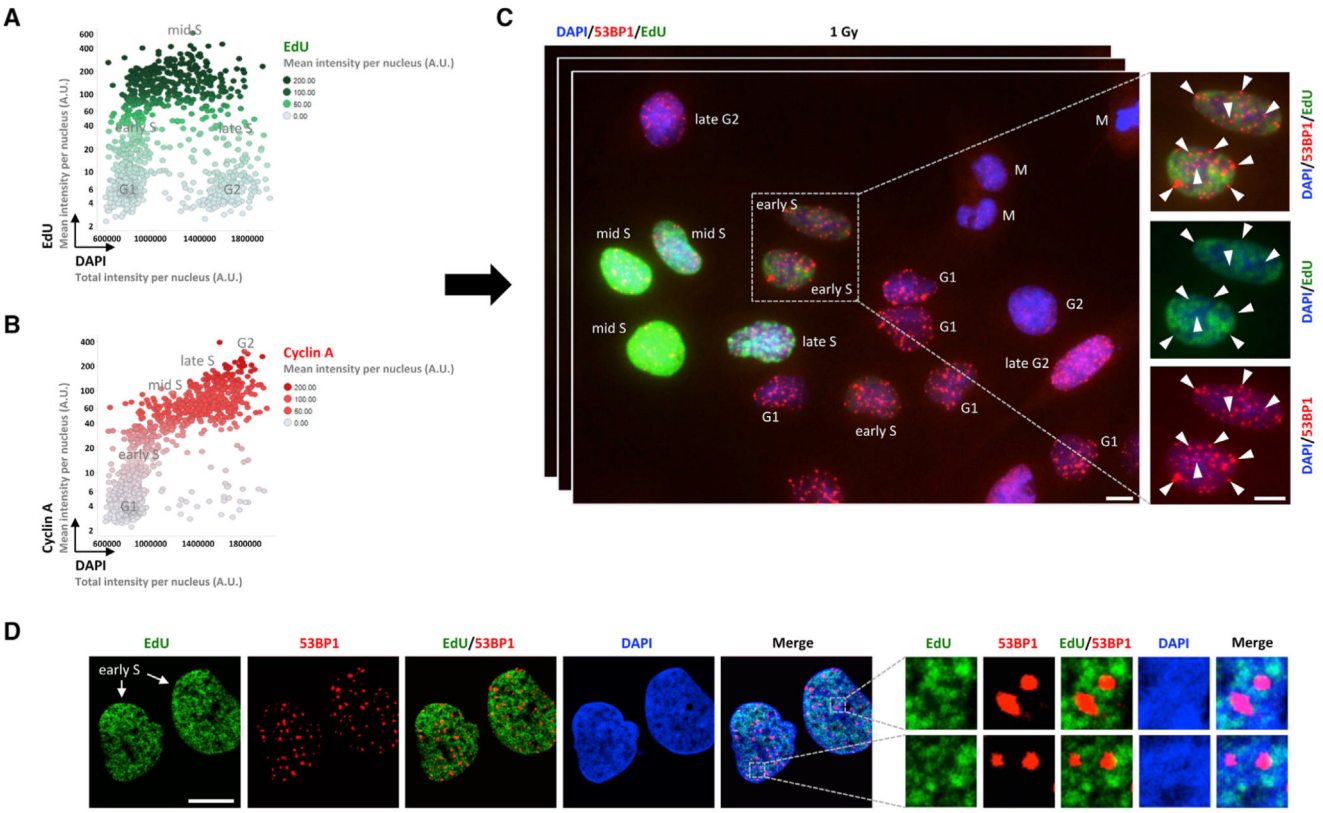

Figure 2. 53BP1 Accumulation Is Excluded from EdU-Marked Replicated Chromatin

(A–C) Cells were pulsed with EdU for 20 min, irradiated with 1 Gy, fixed after 45 min, and stained for EdU, cyclin A, and 53BP1. Multidimensional cell cycle staging based on DAPI/EdU (A) and DAPI/cyclin A (B) was performed. Cell cycle positions were attributed to individual cells accordingly, and overlap between 53BP1 and EdU in early S phase cells was analyzed (C).

(D) Cells were pulsed with EdU, irradiated with 1 Gy, fixed after 45 min, stained for EdU and 53BP1, and analyzed by confocal microscopy. Cells in early S phase were identified by low DAPI/EdU.

Color codes as defined in the figure panels. The scale bars represent 10 μm.

Europe PMC Funders Author Manuscripts

Europe PMC Funders Author Manuscripts

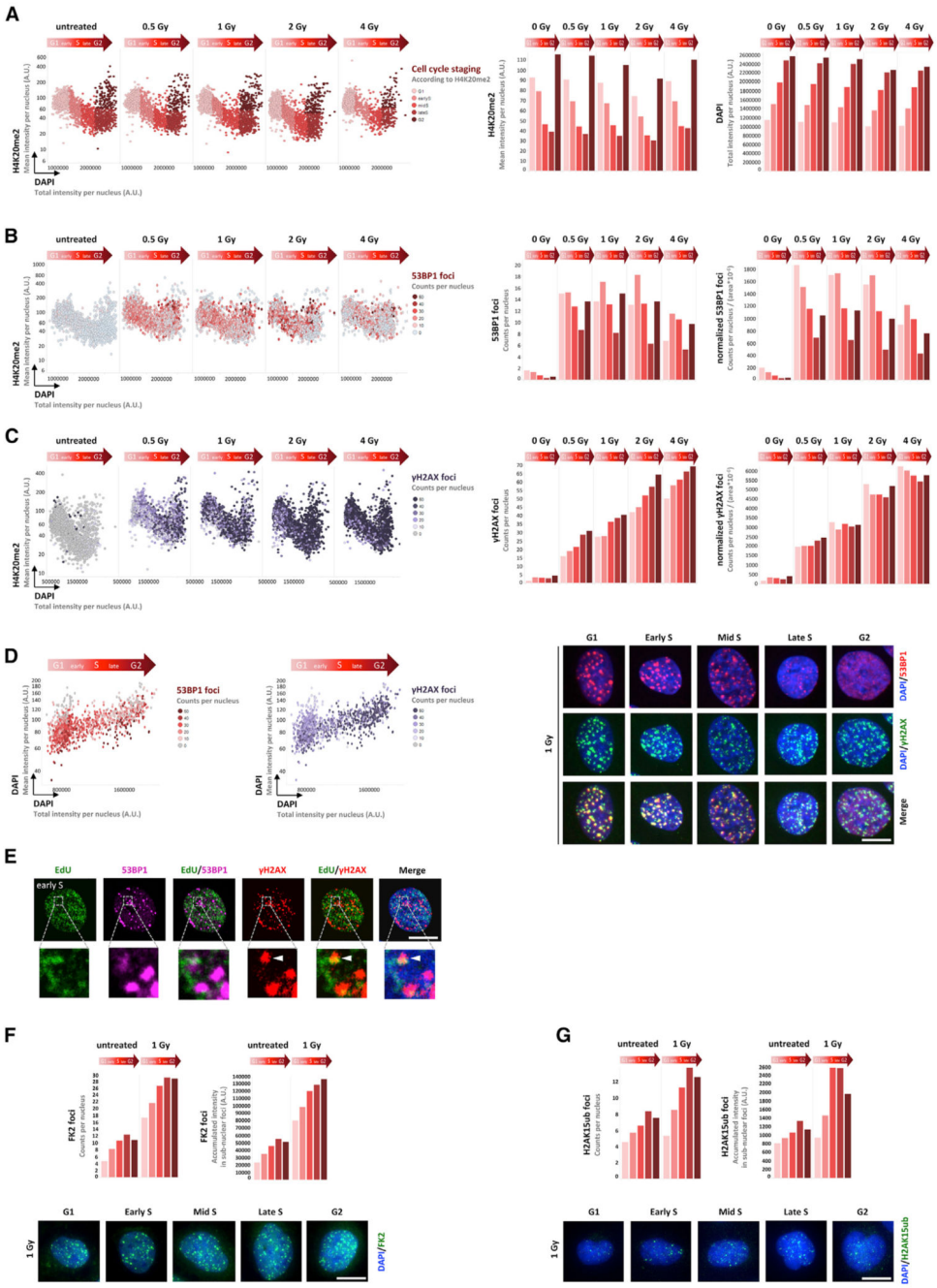

Figure 3. The Discrimination between Pre- and Post-replicative Chromatin Occurs at the Level of 53BP1

(A) Cells were treated with the indicated doses of IR and fixed after 45 min. Cell cycle staging was done based on DAPI and H4K20me2 intensities as indicated.

(B) 53BP1 accumulation into IRIF was quantified and is displayed as a function of cell cycle progression and H4K20me2 levels. Normalization against nuclear area was performed to correct for the cell cycle progression-associated increase in nuclear volume, DNA content, and, presumably, amount of DSBs generated in the genome; see (C).

(C) Cells were treated with IR as indicated and fixed 45 min later, and γH2AX foci were quantified as a function of cell cycle progression and H4K20me2 levels. Note that normalization against nuclear area corrects the cell cycle-related increase in γH2AX foci numbers.
(D) Cells were treated with 1 Gy, fixed 45 min later, and stained for 53BP1 and γH2AX, and 53BP1 and γH2AX foci were quantified as a function of cell cycle progression. Representative images are shown on the right.
(E) Similar to (D), cells were pulsed with EdU, irradiated (1 Gy, 45 min), stained for EdU, 53BP1, and γH2AX, and analyzed by confocal microscopy. Cells in early S phase were identified by low DAPI/EdU.
(F) Cells were treated with IR (1Gy, 45 min), and nuclear foci of ubiquitin conjugates detected by the FK2 antibody were quantified. Representative images are shown below.
(G) Cells were treated with IR as in (F) and nuclear foci of H2AK15ub were quantified. Representative images are shown below.
Color codes as defined in the figure panels. The scale bars represent 10 μm. See also Figures S4 and S5.

Europe PMC Funders Author Manuscripts

Europe PMC Funders Author Manuscripts

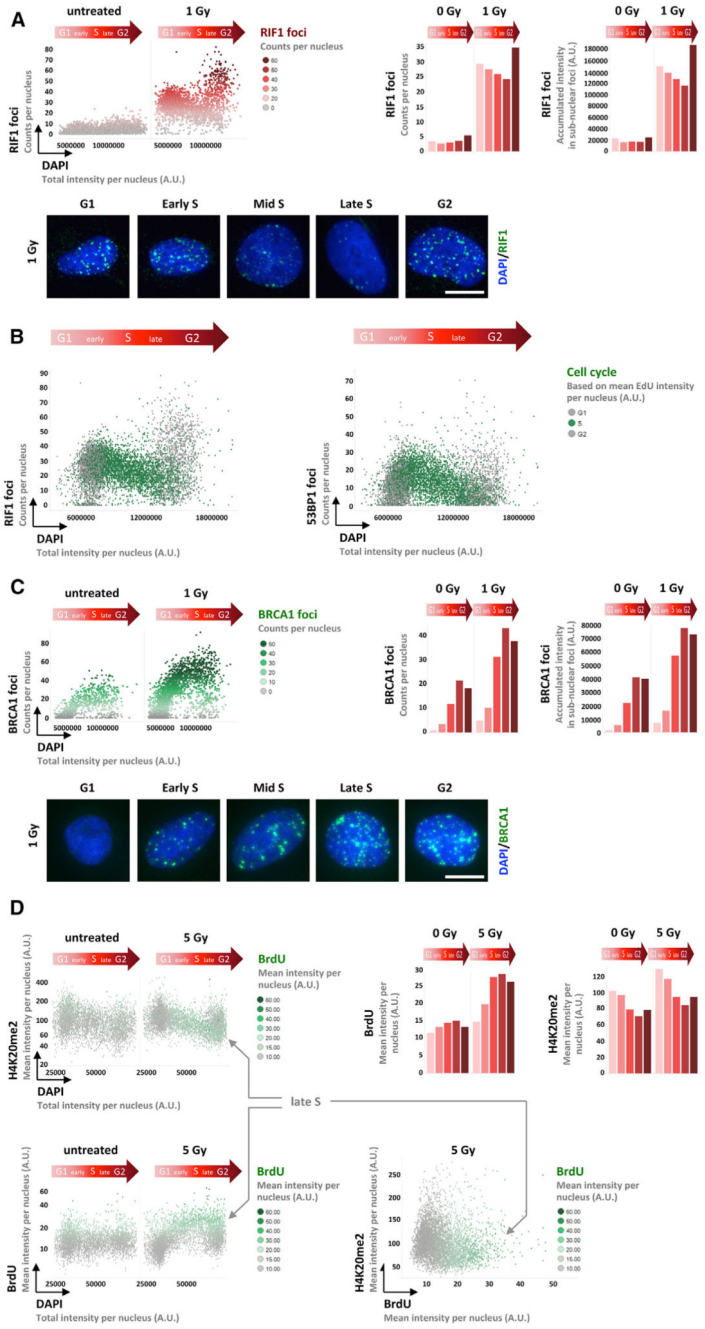

Figure 4. DNA End Resection for HDR Occurs Most Efficiently in Chromatin with Low Levels of H4K20me2

(A) Cells were treated with IR as indicated and fixed 45 min later, and RIF1 foci were quantified and are displayed as a function of cell cycle progression. Representative images are shown below.

(B) EdU-labeled cells were treated with IR (0.5 Gy, 45 min) and co-stained for RIF1 and 53BP1. RIF1 and 53BP1 foci were quantified and are displayed as a function of cell cycle progression.

(C) Cells were treated as in (A), and BRCA1 foci were quantified as a function of cell cycle progression. Representative images are shown below.
(D) Cells were grown in the presence of 10 μM BrdU for 24 h, irradiated with 5 Gy, allowed to recover for 2 h, pre-extracted on ice in 0.2% Triton X-100 for 2 min, and stained for H4K20me2 and BrdU. DNA end resection-associated BrdU signals were quantified as a function of cell cycle progression and H4K20me2 levels.
Color codes as defined in the figure panels. The scale bars represent 10 μm. See also Figure S5.

Europe PMC Funders Author Manuscripts

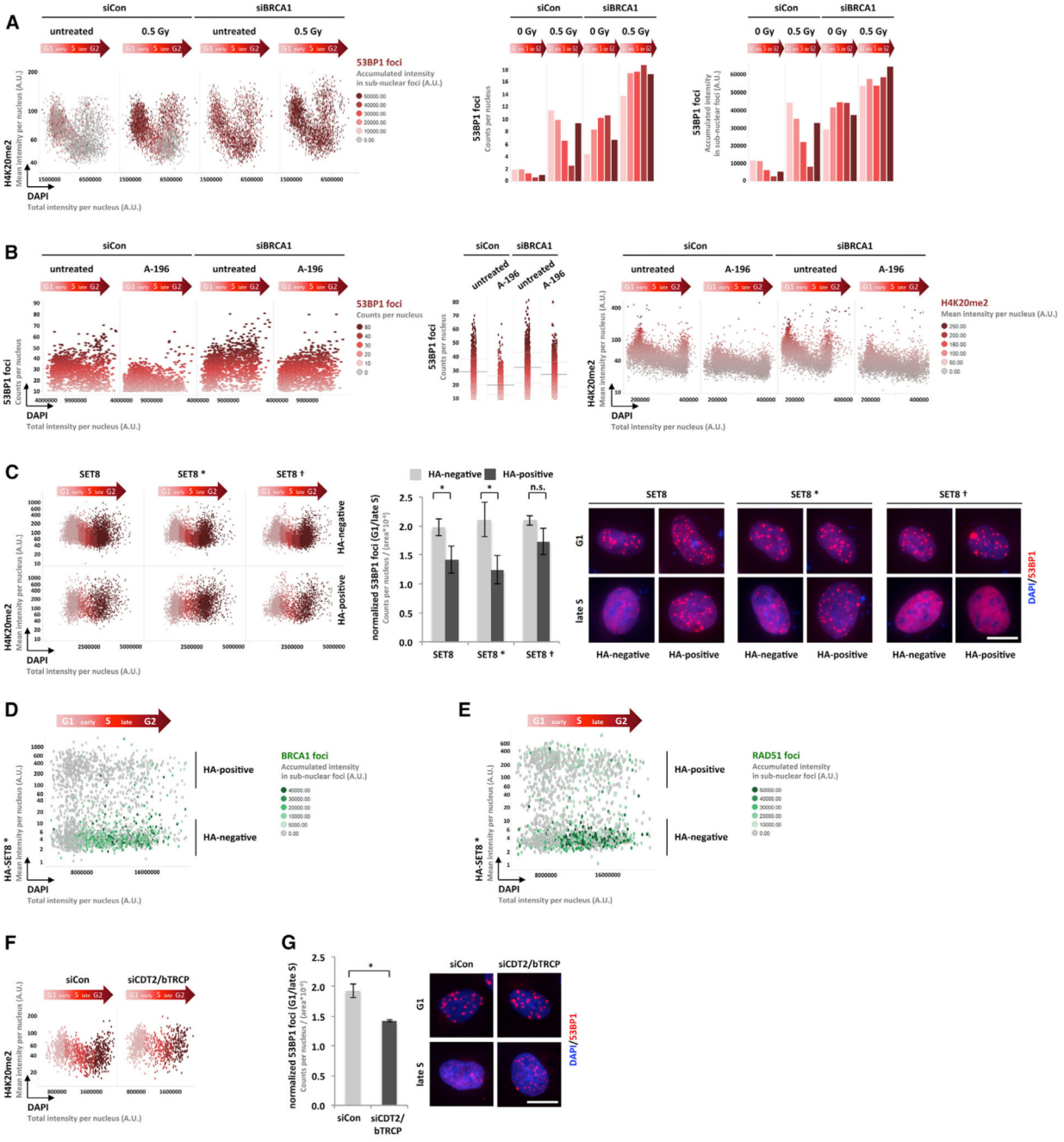

Figure 5. Premature Chromatin Maturation Restores H4K20me2 Levels and Rescues 53BP1 Recruitment in Post-replicative Chromatin

(A) Cells were transfected with negative control siRNA or siRNA against BRCA1, treated with IR (0.5 Gy, 45 min), and stained for H4K20me2 and 53BP1. DAPI/H4K20me2-based cell cycle staging was performed, and 53BP1 foci were quantified and displayed as a function of cell cycle progression and H4K20me2 levels.

(B) Cells were transfected as above in the presence or absence of 1 μM SUV4-20 inhibitor A-196 for 72 hr, irradiated (0.5 Gy, 45 min), and stained for 53BP1 or H4K20me2. 53BP1 foci and H4K20me2 levels are shown as a function of cell cycle progression.

Europe PMC Funders Author Manuscripts

(C) Cells were transfected with wild-type HA-FLAG-SET8, a non-degradable PIP2 version (SET8 *), or a catalytically inactive mutant (SET8 †), and stained for HA and H4K20me2. Cells were gated according to the HA signal and staged according to DAPI intensities. H4K20me2 levels in HA-negative (top) and HA-positive (bottom) cells are displayed as a function of cell cycle progression. Right: cells were transfected with the same set of plasmids, irradiated with 0.5 Gy, fixed 45 min later, and stained for HA and 53BP1. 53BP1 foci in HA-negative and HA-positive cells were quantified and the ratio between 53BP1 foci in G1 cells over late S phase cells was determined. Averages from three independent experiments are shown. Representative images are shown on the right.

(D) Cells were transfected with the non-degradable PIP2 version of SET8 (SET8 *), irradiated with 0.5 Gy, fixed 45 min later, and stained for HA and BRCA1.

(E) Cells were transfected and treated as in (D) and stained for HA and RAD51.

(F) Cells were transfected with negative control siRNA or siRNA against CDT2/bTRCP and stained for H4K20me2. H4K20me2 levels are displayed as a function of cell cycle progression.

(G) Cells were transfected as in (F), irradiated with 0.5 Gy, and fixed 45 min later, and 53BP1 foci were quantified and the ratio between 53BP1 foci in G1 cells over late S phase cells was determined. Averages from three independent experiments are shown. Representative images are shown on the right.

Color codes as defined in the figure panels. Error bars depict SDs. *$p < 0.05$; n.s., not significant ($p \geq 0.05$). The scale bars represent 10 μm. See also Figure S5.

Europe PMC Funders Author Manuscripts

Europe PMC Funders Author Manuscripts

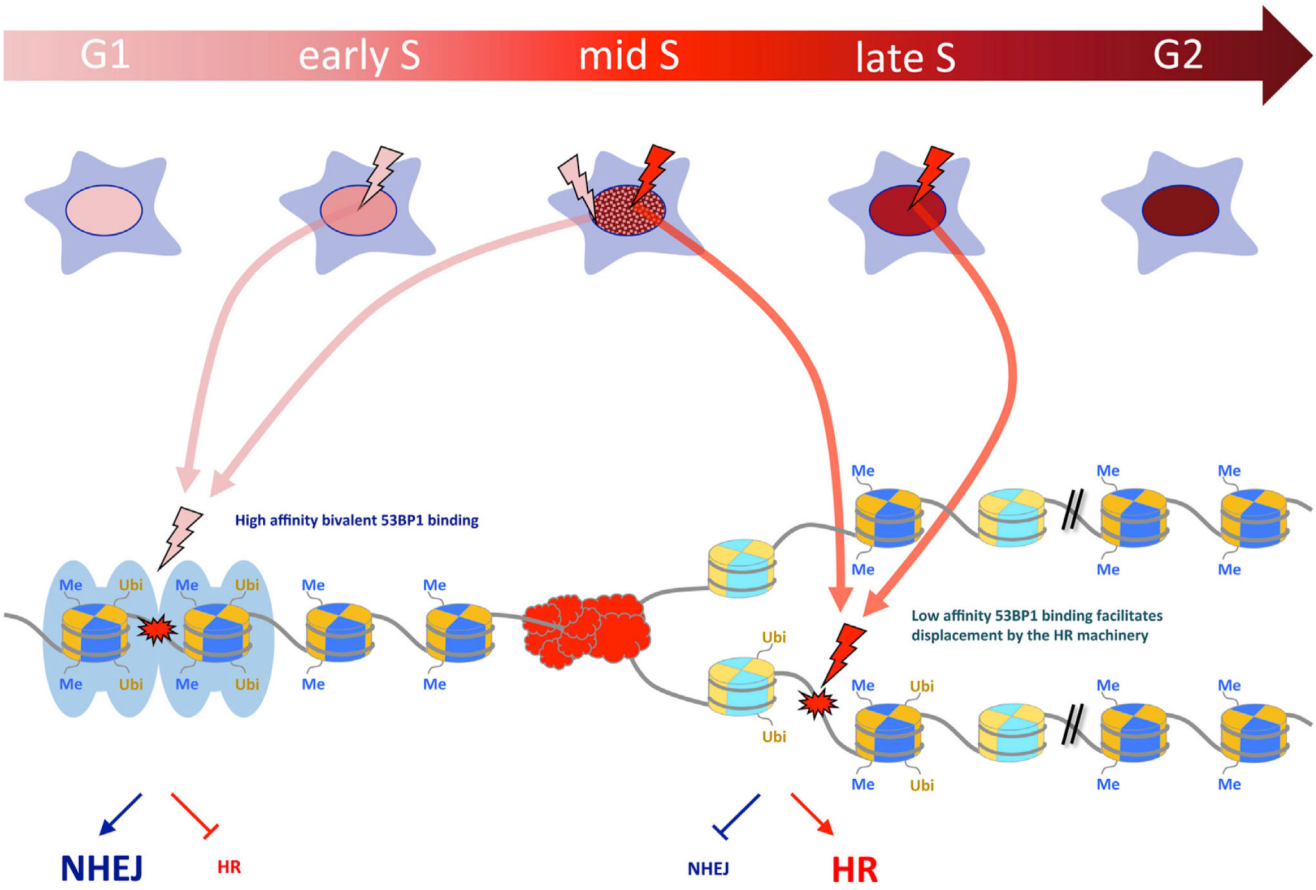

Figure 6. Model for H4K20-Guided DSB Repair Pathway Choice

Replication-coupled dilution of H4K20me2 in nascent chromatin, together with concomitantly increased concentrations of unmethylated H4K20, which helps recruit components of the HDR machinery (Saredi et al., 2016), complement global HDR-promoting signaling events by providing a means to locally discriminate pre- from post-replicative chromatin throughout S phase. DSBs in unreplicated DNA are associated with a high density of H4K20me2, allowing high-affinity bivalent chromatin binding of 53BP1 and its downstream effectors to efficiently inhibit DNA end resection. In contrast, DSBs in replicated DNA are associated with a lower density of H4K20me2 (and higher density of H4K20me0) resulting in a reduced affinity of 53BP1, thus lowering the threshold for its displacement by the HR machinery.